Examining the Properties of Low-luminosity Hosts of Type Ia Supernovae from ASAS-SN

Thomas W.-S. Holoien[1,20] , Vera L. Berger[1,2] , Jason T. Hinkle[3] , L. Galbany[4,5] , Allison L. Strom[6,7] , Patrick J. Vallely[8],
Joseph P. Anderson[9] , Konstantina Boutsia[10], K. D. French[11] , Christopher S. Kochanek[8,12,21] , Hanindyo Kuncarayakti[13,14] ,
Joseph D. Lyman[15] , Nidia Morrell[10] , Jose L. Prieto[16,17] , Sebastián F. Sánchez[18] , K. Z. Stanek[8,12], and
Gregory L. Walth[19]

[1] The Observatories of the Carnegie Institution for Science, 813 Santa Barbara St., Pasadena, CA 91101, USA; tholoien@carnegiescience.edu
[2] Department of Physics and Astronomy, Pomona College, 333 N. College Way, Claremont, CA 91711, USA
[3] Institute for Astronomy, University of Hawaíi, 2680 Woodlawn Drive, Honolulu, HI 96822, USA
[4] Institute of Space Sciences (ICE, CSIC), Campus UAB, Carrer de Can Magrans, s/n, E-08193 Barcelona, Spain
[5] Institut d'Estudis Espacials de Catalunya (IEEC), E-08034 Barcelona, Spain
[6] Department of Astrophysical Sciences, Princeton University, 4 Ivy Lave, Princeton, NJ 08544, USA
[7] Department of Physics and Astronomy and Center for Interdisciplinary Exploration and Research in Astrophysics (CIERA), Northwestern University, 2145 Sheridan
Road, Evanston, IL 60208, USA
[8] Department of Astronomy, The Ohio State University, 140 West 18th Avenue, Columbus, OH 43210, USA
[9] European Southern Observatory, Alonso de Córdova 3107, Casilla 19, Santiago, Chile
[10] Las Campanas Observatory, Carnegie Observatories, Casilla 601, La Serena, Chile
[11] Department of Astronomy, University of Illinois, 1002 W. Green St., Urbana, IL 61801, USA
[12] Center for Cosmology and AstroParticle Physics (CCAPP), The Ohio State University, 191 W. Woodruff Ave., Columbus, OH 43210, USA
[13] Tuorla Observatory, Department of Physics and Astronomy, FI-20014 University of Turku, Finland
[14] Finnish Centre for Astronomy with ESO (FINCA), FI-20014 University of Turku, Finland
[15] Department of Physics, University of Warwick, Coventry, CV4 7AL, UK
[16] Núcleo de Astronomía de la Facultad de Ingeniería y Ciencias, Universidad Diego Portales, Av. Ejército 441, Santiago, Chile
[17] Millennium Institute of Astrophysics, Santiago, Chile
[18] Instituto de Astronomía, Universidad Nacional Autónoma de Mexico, A.P. 70-264, C.P. 04510, México, D.F., Mexico
[19] IPAC, California Institute of Technology, Mail Code 314-6, 1200 E. California Blvd., Pasadena, CA 91125, USA

Abstract

We present a spectroscopic analysis of 44 low-luminosity host galaxies of Type Ia supernovae (SNe Ia) detected by the All-Sky Automated Survey for Supernovae (ASAS-SN), using hydrogen, oxygen, and sulfur emission lines to measure metallicities and star formation rates. We find no statistically significant evidence that the star formation activity and metallicities of the galaxies in our sample are inconsistent with galaxies of similar luminosities and masses. We identify two 3σ outlier galaxies that have high metallicities for their stellar masses, but find that their other properties are consistent with general galaxies. The overall consistency between our sample and general galaxy samples further strengthens the evidence from more luminous SN Ia host galaxy samples that SN Ia host galaxies are typical.

Unified Astronomy Thesaurus concepts: Type Ia supernovae (1728); Supernovae (1668); Galaxy abundances (574)

Supporting material: data behind figure, machine-readable tables

1. Introduction

Type Ia supernovae (SNe Ia) are some of the most energetic events in the Universe, and due to the empirical relations between their intrinsic brightness and other properties, such as decline rate and color (e.g., Phillips 1993; Hamuy et al. 1996), they can be used as standardizable candles to measure cosmological distances. SNe Ia were crucial to the discovery of the accelerating expansion of the Universe (Riess et al. 1998; Perlmutter et al. 1999). SNe Ia are also useful probes of physics under extreme conditions, are an end stage of stellar evolution, and can significantly impact the evolution of their host galaxy environments (e.g., Maoz et al. 2012; Nomoto et al. 2013; Maoz & Graur 2017). The study of these events thus impacts our understanding of a wide variety of astronomical subfields.

Despite all this, the progenitor systems of SNe Ia are still not known, and their physics are not fully understood (e.g., Shappee et al. 2017, 2018, 2019; Vallely et al. 2019; Tucker et al. 2020). There is also diversity in SNe Ia, with subtypes exhibiting different luminosities and decline rates that must be accounted for in order to measure their distances accurately (e.g., Filippenko et al. 1992b, 1992a; Phillips et al. 1992; Leibundgut et al. 1993; Foley et al. 2013).

One way to study the physical causes of the differences in SN Ia properties and the possible dependence of these differences on progenitor properties is to study the environments of SNe Ia. Previous studies of SNe Ia and their host galaxies have revealed correlations between the brightness, decline rate, and expansion rate of SNe Ia and the morphology, mass, metallicity, star formation rate (SFR), specific star formation rate (sSFR), and color of their host galaxies (e.g., Filippenko 1989; Branch & van den Bergh 1993; Hamuy et al. 2000; Gallagher et al. 2005, 2008; Howell et al. 2009; Lampeitl et al. 2010; Sullivan et al. 2010; Uddin et al. 2017, 2020; Kim et al. 2019; Smith et al. 2020; Kelsey et al. 2021; Ponder et al. 2021; Popovic et al. 2021). These correlations also hold, and are typically stronger, when examining the local environments around SNe, as

---

[20] NHFP Einstein Fellow.
[21] Radcliffe Fellow.

opposed to global galaxy properties (e.g., Rigault et al. 2013, 2015, 2020; Anderson et al. 2015; Jones et al. 2015, 2018; Moreno-Raya et al. 2016a, 2016b; Galbany et al. 2018; Kim et al. 2018, 2019; Roman et al. 2018; Rose et al. 2019; Kelsey et al. 2021). This implies that one or more properties of SN Ia progenitors that are correlated with host galaxy properties are responsible for some of the observed diversity in SN Ia light curves.

Previous studies of the properties of SN Ia host galaxies have found that SN Ia hosts are generally consistent with the general population of galaxies. In particular, Childress et al. (2013) performed both a photometric and spectroscopic study of SN Ia hosts using the sample from the Nearby Supernova Factory (Aldering et al. 2002). They found that SN Ia hosts had star formation activity and metallicities representative of normal galaxies, as had been found in previous work on photometric properties, such as mass (e.g., Howell et al. 2009; Neill et al. 2009). These and earlier studies of SN Ia hosts largely focused on higher-mass, higher-luminosity host galaxies. This is likely a byproduct of earlier SN surveys being biased toward certain types of hosts due to observing strategy and/or survey design, and by a lack of follow-up resources to observe fainter, low-luminosity host galaxies in significant numbers.

In recent years, the proliferation of large-area, rapid-cadence surveys, such as the All-Sky Automated Survey for Supernovae (ASAS-SN; Shappee et al. 2014), the Asteroid Terrestrial-impact Last Alert System (Tonry et al. 2018), and the Zwicky Transient Facility (Bellm et al. 2019), has resulted in large samples of SNe free from many of the host-dependent biases of earlier SN surveys. This has allowed SN properties and rates to be correlated with host properties at much broader ranges than were previously possible. For example, Brown et al. (2019) used the ASAS-SN sample to extend the observed trend in the specific SN Ia rate with respect to host galaxy mass to roughly three orders of magnitude lower in mass than in Kistler et al. (2013), who used the Lick Observatory Supernova Search (Li et al. 2000) sample. These modern samples, particularly nearby ones from bright-sky surveys, such as ASAS-SN, are thus ideal for examining SN Ia host galaxies at low luminosities and masses. We can use these samples to test whether these hosts are similar to the general population of galaxies, as has been seen with higher-mass and higher-luminosity hosts.

This is important to test for multiple reasons. First, if low-luminosity and low-mass SN Ia hosts differ from typical galaxies, this may affect the progenitors and properties of SNe Ia in these galaxies. Understanding how the SNe Ia in these hosts may differ from those in more typical hosts will be important for developing a full physical understanding of SNe Ia and their explosion mechanisms. Second, if these low-luminosity hosts do not have properties similar to general galaxies, it would mean that standard galaxy relations, e.g., the mass–metallicity relation, would not apply to this population of galaxies. Properties such as metallicity, which can only reliably be measured using observationally expensive spectroscopy, are often inferred based on photometrically measurable properties, such as mass, when studying SN Ia hosts (e.g., Howell et al. 2009; Neill et al. 2009). If low-luminosity and low-mass hosts deviate from standard relations, it is crucial to understand how they deviate, so that we can correctly account for the differences when inferring properties such as metallicity in these galaxies.

This paper presents a spectroscopic study of the properties of 44 low-luminosity SN Ia host galaxies selected from the first 3

yr of ASAS-SN. In Section 2, we discuss the galaxies in our sample and how they were selected, the spectroscopic data set, how we measured the emission line fluxes from the spectra, and how we translated these line fluxes into physical properties. In Section 3, we analyze these properties and compare them to several samples of non-SN host galaxies. Finally, in Section 4, we discuss our findings and the future directions of this work. Throughout this paper, we assume a standard ΛCDM cosmology, with $H_0 = 69.6$ km s^{-1} Mpc^{-1}, $\Omega_M = 0.296$, and $\Omega_\Lambda = 0.714$ (Wright 2006; Bennett et al. 2014).

2. Low-luminosity SN Ia Host Galaxy Sample

2.1. Sample Details

To select a representative sample of low-luminosity host galaxies of SNe Ia, we first started with the sample of SN Ia used by Brown et al. (2019) to measure the relative specific SN Ia rate from the first 3 yr of ASAS-SN. The ASAS-SN sample is ideal for a number of reasons: ASAS-SN surveys the entire sky systematically, meaning there is no bias toward a previously selected sample of galaxies or toward galaxies of a particular luminosity; ASAS-SN surveys the nearby Universe, meaning low-luminosity galaxies in the ASAS-SN sample should be close enough to observe spectroscopically; and the ASAS-SN sample was small enough for all possible SNe to be observed spectroscopically, lowering the likelihood of an SN being missed due to limited resources.

From the Brown et al. (2019) sample we selected galaxies with $\log L/L_\star \leqslant -1.5$, calculating the luminosity of the galaxies based on the K_S-band magnitudes from Holoien et al. (2017a) and assuming $M_{\star,K_S} = -24.2$ (Kochanek et al. 2001). This resulted in a sample of 58 low-luminosity SN Ia host galaxies that we targeted for spectroscopic observation. The final sample presented here comprises 44 of these galaxies, for which we were able to obtain spectra with high enough signal-to-noise ratios (S/Ns) to measure the emission line fluxes needed for our analyses. These are primarily Hα, Hβ, the [O III] λ4959/5007 doublet, and the [N II] λ6548/6583 doublet, though we also measure several others when possible. Our reduced spectra are available in the online journal. For completeness, the spectra available online also include the reduced spectra of nine additional galaxies that were observed, but are not included in our analyses, as they did not yield well-measured emission line fluxes.

Figure 1 shows histograms of the redshifts, stellar masses, and luminosities of the galaxies in our sample compared to the full sample from Brown et al. (2019). Our sample is composed of the majority of the lower-mass and lower-luminosity galaxies in their sample. The low-mass and low-luminosity galaxies from the Brown et al. (2019) sample that are not included in our sample are largely ones that were selected by our luminosity cut, but were too faint to obtain spectra with well-measured emission line fluxes. The redshifts in our sample are distributed similarly to the overall Brown et al. (2019) sample, with redshifts of $z \leqslant 0.05$.

The telescopes and instruments used to obtain the spectra for our sample were: (1) the Inamori–Magellan Areal Camera and Spectrograph (IMACS; Dressler et al. 2011) on the 6.5 m Magellan–Baade telescope; (2) the Low-Dispersion Survey Spectrograph 3 (LDSS-3) on the 6.5 m Magellan Clay telescope; (3) the Multi-Object Double Spectrograph (MODS; Pogge et al. 2010) on the dual 8.4 m Large Binocular Telescope (LBT); (4) the
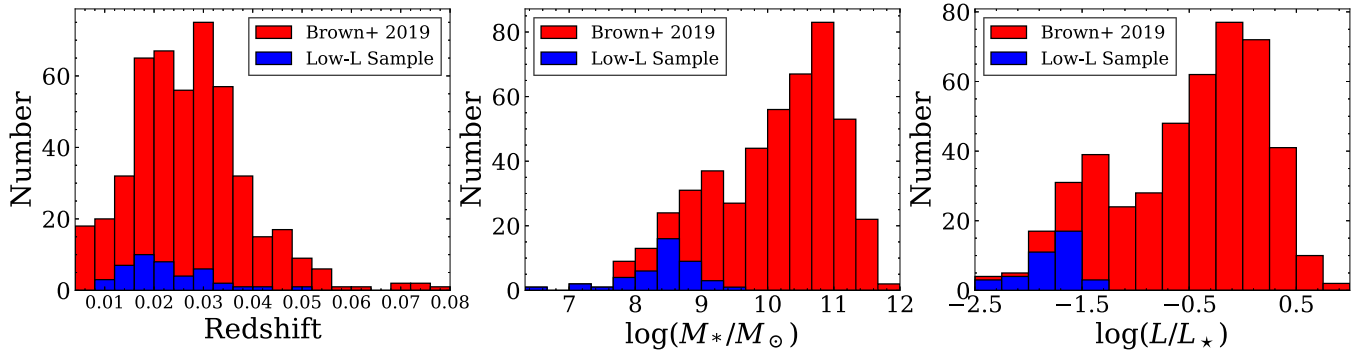
Figure 1. Histograms of the redshifts (left panel), stellar masses (middle panel), and luminosities (right panel) for the low-luminosity host galaxy sample presented in this paper (blue) and the full SN Ia host galaxy sample from Brown et al. (2019; red). Stellar mass is shown in Solar masses and the luminosity is relative to $L_\star$, assuming $M_{\star,K_S} = -24.2$ (Kochanek et al. 2001).

Multi-Unit Spectroscopic Explorer (MUSE; Bacon et al. 2014), located at the Nasmyth B focus of Yepun, the Very Large Telescope UT4 telescope at Cerro Paranal Observatory; and (5) the Potsdam Multi-Aperture Spectrograph (PMAS; Roth et al. 2005) mounted on the 3.5 m telescope of the Centro Astronómico Hispano Alemán at the Calar Alto Observatory. With the exception of the MUSE and PMAS spectra, these spectra consisted of longslit spectra obtained at the parallactic angle and centered on the host nucleus, with total integration times typically between 1 and 4 hr. We chose to center our spectra on the host nuclei, as the majority of the galaxies in our sample are either too small to differentiate the location of the SN from the host nucleus or too diffuse to obtain a high-S/N spectrum at the SN location.

We used IRAF to reduce our IMACS and LDSS-3 spectra following standard procedures, including bias subtraction, flat-fielding, one-dimensional spectral extraction, and wavelength calibration using a comparison lamp spectrum. The MODS spectra were reduced using the MODS spectroscopic pipeline.[22] We flux-calibrated our spectra using observations of spectro-photometric standard stars obtained on the same nights as our galaxy spectra.

Seven of the spectra in our sample were obtained with MUSE. Its modular structure is composed of 24 identical integral field unit (IFU) modules that together sample, in Wide Field Mode, a near-contiguous 1 arcmin^2 field of view (FOV) with spaxels of $0\farcs2 \times 0\farcs2$, a wavelength coverage of 4650 Å–9300 Å, and a mean resolution of $R \sim 3000$. This produces $\sim 100,000$ spectra per pointing. These observations were obtained by the All-weather MUSE Supernova Integral field of Nearby Galaxies[23] (Galbany et al. 2016; L. Galbany et al. 2023, in preparation) survey. This survey has been running for 10 semesters and has compiled observations for more than 600 nearby SN host galaxies.

One additional spectrum (UGC 08503) was obtained with PMAS in PPak mode (Verheijen et al. 2004; Kelz et al. 2006). PPak consists of a fiber bundle of 382 fibers with $2\farcs7$ diameter, 331 of which are ordered in a single hexagonal bundle, with the remaining fibers being used for sky measurements and calibration purposes. Observations were performed using the V500 grating, which has a spectral resolution of ~ 6 Å over the wavelength range 3750 Å–7300 Å. The final product is a three-dimensional data cube with a 100% covering factor within a hexagonal FOV of ~ 1.3 arcmin^2 with $1'' \times 1''$ pixels, which

correspond to ~ 4000 spectra per object. This observation is part of the PMAS/PPak Integral field Supernova hosts COmpilation (PISCO;[24] Galbany et al. 2018), a project that aimed at building a sample of SN host galaxies for environmental studies (Galbany et al. 2014, 2016). As of 2022 May, the PISCO sample contained 363 galaxies.

To extract the global spectra of the host galaxies from the MUSE and PMAS data, we defined an elliptical aperture by fitting an elliptical Sérsic profile to the galaxy light, using an image obtained by compressing the cube in the wavelength direction, simulating an image with a flat filter from ~ 4800 Å to ~ 9300 Å. Circular apertures were placed at the positions of foreground stars selected from the Gaia Early Data Release 3 catalog (Gaia Collaboration et al. 2021), and the flux within the apertures was removed and interpolated from the nearby pixels outside the aperture.

2.2. Line Measurements

In order to calculate the metallicities and SFRs of the galaxies in our sample, we first measured the fluxes of the emission lines in the spectra. To do so, we used the Python code PPXF (Cappellari 2012, 2017) to simultaneously fit the stellar background needed to model the effects of stellar absorption lines and the emission line fluxes. PPXF uses the Penalized Pixel-Fitting method (Cappellari & Emsellem 2004; Cappellari 2017) to extract the galaxy stellar and gas kinematics, stellar population, and gas emission lines, by fitting a set of templates to an observed spectrum. After fitting a stellar template to the observed spectrum, PPXF subtracts the template from the spectrum and fits Gaussian profiles to each of the emission lines. Each line is fit individually, with the exceptions of the [O III] $\lambda4959/5007$, [O I] $\lambda6300/6364$, and [N II] $\lambda6548/6583$ doublets, where the brighter of the two lines are fit and the lines are assumed to have a 3:1 flux ratio.

We obtained line fluxes by integrating the Gaussian model of each emission component. We calculated equivalent widths for Hα and Hβ by estimating the continuum using regions near the lines in the observed spectrum (prior to the PPXF template subtraction) and dividing the measured line flux by the continuum estimate. An example host galaxy spectrum, the best-fit stellar template, and the combined stellar template + emission lines model are shown in Figure 2. The PPXF emission line models are shown in gray.

---

[22] http://www.astronomy.ohio-state.edu/MODS/Software/modsIDL/
[23] https://amusing-muse.github.io/
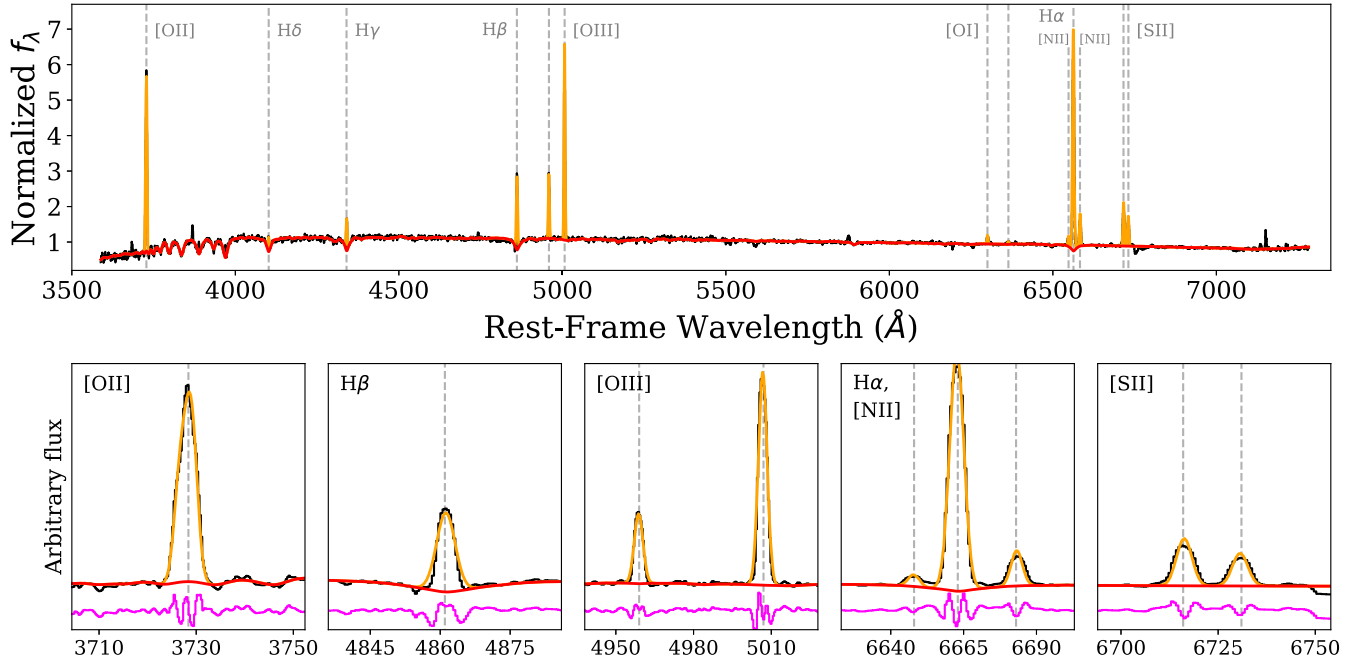[24] https://github.com/lgalbany/pisco

Figure 2. The MODS/LBT data of the galaxy 2MASX J03051061+3754003, the host of the supernova ASASSN-15li, and fits from PPXF. The black curve is the observed spectrum, the red curve is the stellar continuum fit, and the gold curve is the combined stellar continuum + emission line fit. The lines included in the fit are marked and labeled in gray. The lower panels show zoomed-in views of several fitted lines, as well as the residual difference between the data and the combined model in magenta. The labels in the upper left corners give the lines being shown in each panel.

(The data used to create this figure are available.)

Table 1
Emission Line Fluxes of Our Low-L SN Ia Host Galaxy Sample

	Galaxy Name[a]			
Line	2MASX J03051061+3754003	AGC 331536	APMUKS(BJ) B032028.93−441621.0	CGMW 2-2125
[O II] $\lambda3727 + 3729$	5748.0 ± 212.4	78.63 ± 6.53	⋯	⋯
Hδ	98.07 ± 12.1	4.49 ± 0.49	156.7 ± 9.68	29.7 ± 18.3
Hγ	489.7 ± 19.28	8.54 ± 0.72	309.2 ± 13.92	30.64 ± 17.45
Hβ	1263.0 ± 36.57	21.65 ± 1.4	714.9 ± 24.89	71.91 ± 30.22
[O III] $\lambda4959$	1071.0 ± 29.22	14.44 ± 0.89	635.8 ± 20.89	32.3 ± 12.98
[O III] $\lambda5007$	3170.0 ± 85.39	43.15 ± 2.62	1889.0 ± 61.3	95.02 ± 37.71
[O I] $\lambda6300$	124.9 ± 8.1	2.27 ± 0.45	24.09 ± 6.8	11.46 ± 7.16
[O I] $\lambda6364$	41.2 ± 2.66	0.75 ± 0.15	7.98 ± 2.24	3.78 ± 2.34
[N II] $\lambda6548$	142.5 ± 3.78	2.85 ± 0.19	84.94 ± 3.04	17.06 ± 5.27
Hα	3608.0 ± 71.15	61.89 ± 2.75	2043.0 ± 48.56	205.3 ± 58.61
[N II] $\lambda6583$	425.8 ± 11.24	8.52 ± 0.58	253.7 ± 9.03	50.82 ± 15.6
[S II] $\lambda6716$	567.2 ± 13.39	10.39 ± 0.65	323.3 ± 10.34	92.75 ± 26.35
[S II] $\lambda6731$	388.0 ± 10.82	9.2 ± 0.62	218.9 ± 8.77	21.98 ± 8.77
Hα EW (Å)	41.07 ± 0.1	19.18 ± 0.13	96.76 ± 0.31	11.32 ± 0.35
Hβ EW (Å)	8.51 ± 0.07	4.71 ± 0.08	16.74 ± 0.16	2.32 ± 0.27

Notes. Extinction-corrected line fluxes and equivalent widths for the galaxies in our sample. The line fluxes were calculated using PPXF and corrected for extinction using the Balmer decrement, as described in Section 2.2. All fluxes are given in units of 10^{-17} erg s^{-1} cm^{-2} and equivalent widths are given for Hα and Hβ in Å. A portion of the table is shown here for guidance regarding its form and content; the full table is available in machine-readable format in the online journal.
[a] For cases where a galaxy has not been previously cataloged by any survey, and thus does not have an archival name or designation, we use "Uncatalogued" for the name and give the corresponding SN name in parentheses.

(This table is available in its entirety in machine-readable form.)

Finally, we estimated the dust extinction in each galaxy by comparing the Balmer decrement (Hα/Hβ) to the expected value of 2.86 for Case B recombination (Osterbrock 1989). Roughly 29% of the galaxies in our sample have Balmer decrements consistent with the Case B ratio within 3σ. We assume zero extinction for the three galaxies in our sample with Hα/H$\beta < 2.86$. We then calculate $E(B-V)$ and correct the flux of each spectroscopic line for extinction using the same Cardelli et al. (1989) $R_V = A(V)/E(B-V) = 3.1$ extinction law used in other studies of low-luminosity galaxies. Our final extinction-corrected line fluxes and equivalent widths are presented in Table 1.
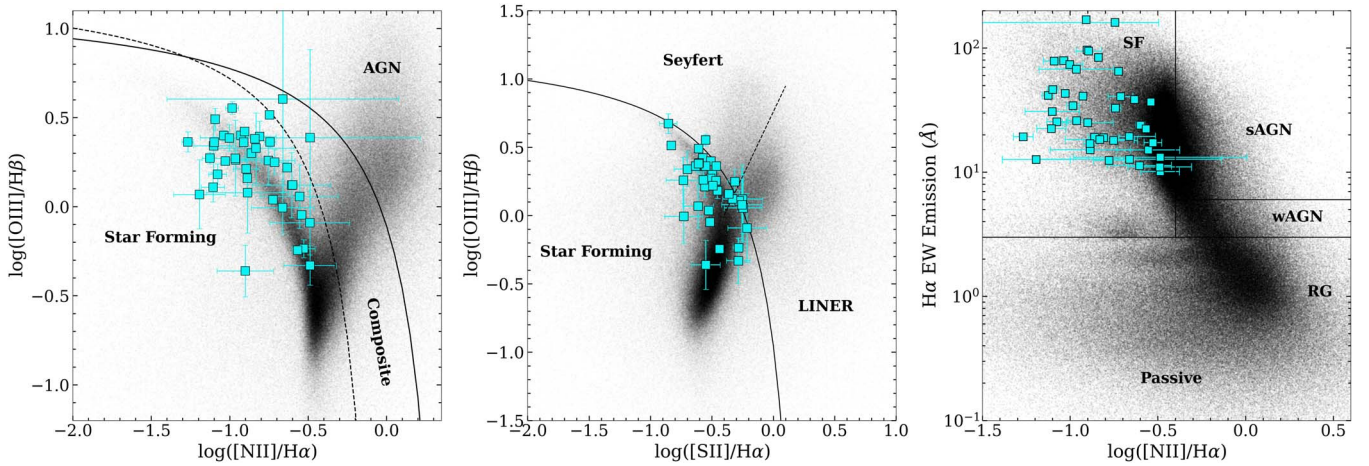
Figure 3. Emission line diagnostic diagrams for our sample (blue squares). Left panel: BPT diagram showing log([O III] / Hβ) vs. log([N II] / Hα) (Baldwin et al. 1981; Veilleux & Osterbrock 1987). The solid line shows the separation between AGNs (above) and H II/star-forming regions (below), based on theoretical models (Kewley et al. 2001), while the dotted line shows the same classifications based on empirical models (Kauffmann et al. 2003). Center panel: log([O III] / Hβ) vs. log([S II] / Hα) diagnostic from Veilleux & Osterbrock (1987). The solid line separates AGNs from H II regions, as in the BPT diagram (Kewley et al. 2001), and the diagonal dashed line separates Seyferts (above) and LINERs (below; Kewley et al. 2006). Right panel: Hα emission line equivalent width (EW$_{\mathrm{H}\alpha}$) compared to log([N II] / Hα), also called the WHAN diagram (Cid Fernandes et al. 2011). Lines separating star-forming galaxies (SF), strong AGNs (sAGN), weak AGNs (wAGN), and passive/"retired galaxies" (RG) are shown (Cid Fernandes et al. 2011). In all panels, galaxies from SDSS DR8 (Eisenstein et al. 2011) are shown in black.

In Figure 3, we show several line diagnostic diagrams with our low-luminosity host sample compared to the Sloan Digital Sky Survey Data Release 8 (SDSS DR8; Eisenstein et al. 2011) sample of galaxies. The left panel shows the Baldwin–Phillips–Terlevich diagram (BPT diagram; Baldwin et al. 1981), the center panel shows the log([S II]/Hα) versus log([O II]/Hβ) diagram (Veilleux & Osterbrock 1987), and the right panel shows the WHAN (Hα equivalent width versus [N II]/Hα) diagram (Cid Fernandes et al. 2011). Lines dividing different types of galaxies (typically star-forming versus active galactic nucleus, or AGN) are shown in each panel and described in the figure caption. In all three cases, the vast majority of the galaxies in our sample clearly lie in the star-forming or H II regions of the diagrams, although a few fall in the "Composite" region of the BPT diagram or the Seyfert region of the [S II]/Hα diagram. Our sample is largely clustered in a region of the BPT diagram that is populated by low-mass star-forming galaxies, which reinforces the low-mass nature of our sample (see Section 2.3). Given the strong emission lines present in our spectra and the low-luminosity, low-mass nature of the sample, their locations in these diagnostic figures are unsurprising.

2.3. Physical Properties

The analyses presented here primarily consider four physical properties of our galaxies: the stellar mass, the metallicity, the SFR, and the sSFR. Stellar masses for the galaxies were calculated by Brown et al. (2019). They computed masses for the galaxies using Fitting and Assessment of Synthetic Templates (FAST; Kriek et al. 2009) to fit spectral energy distributions (SEDs) to archival photometry of the galaxies. The archival photometry included GALEX *NUV*, SDSS or Panoramic Survey Telescope and Rapid Response System (Pan-STARRS) optical, Two Micron All Sky Survey (2MASS) *JHK$_S$*, and Wide-field Infrared Survey Explorer (WISE) *W*1 and *W*2 data, or a subset thereof when reliable magnitudes were not available for all bands. Their fits assumed a Cardelli et al. (1989) extinction law with $R_V = 3.1$, Galactic extinctions from Schlafly & Finkbeiner (2011), and used an exponentially declining star formation history, a Salpeter (1955) initial mass function (IMF),

and the Bruzual & Charlot (2003) stellar population models for the fits. Due to the heterogenous photometry used for the fit, they assumed a minimum uncertainty of 0.1 mag for all magnitudes, in order to avoid the fit being biased by artificially small uncertainties in a given filter. A comparison of their results with the values from the Max Planck Institute for Astrophysics and the Johns Hopkins University (MPA-JHU) Galspec pipeline (Kauffmann et al. 2003) indicated that the masses they derive are largely consistent with those from Galspec, and we adopt the Brown et al. (2019) masses in our analyses.

One galaxy in our sample, the uncatalogued host of CSS141227:132741−111252, was not included in the Brown et al. (2019) analysis, as it was previously not detected in archival data. We obtained *grizy* Kron magnitudes of the host from Pan-STARRS (Chambers et al. 2016; Flewelling et al. 2020) and infrared *W*1 and *W*2 magnitudes from the WISE (Wright et al. 2010, 2019) AllWISE catalog and fit the SED using FAST in the same manner as Brown et al. (2019). We find that the host has a stellar mass of $M_\star = (1.35^{+0.06}_{-0.03}) \times 10^8\, M_\odot$, consistent with a dwarf galaxy and similar to many galaxies in our sample. One additional galaxy in our sample, GALEXASC J134316.80−313318.2, has limited archival data available with which to fit the SED, and only has an upper limit on its mass in Brown et al. (2019). We use the same limit here.

Translating emission line fluxes into gas-phase metallicities is highly dependent on the choice of calibration, with different calibrations often disagreeing by as much as ~0.5 dex (e.g., Kewley & Ellison 2008). Further, metallicity calibrations are only valid for specific ranges of line ratios or metallicities and/ or based on different estimates of physical properties that correlate with metallicity. Finding a single method that can be used for a wide range of metallicities is difficult. Empirical metallicity calibrations are generally preferred, as they are based on the electron temperature abundance scale, but they are typically calculated based on samples that do not cover the full range of galaxy parameter space.

We calculate gas-phase metallicities for the galaxies in our sample using the empirical calibrations derived by Curti et al.

(2017). Curti et al. (2017) calculated a new set of empirical metallicity calibrations using a uniform application of the T_e method across the full metallicity range spanned by SDSS galaxies. Their calibrations span more than 1 dex in metallicity, have been calculated for several commonly used line ratios, and the calibrations for different line ratios are consistent with one another to within 0.05 dex. They are ideal for both our low-luminosity SN host galaxy sample and the comparison samples we use (see Section 3 below).

We use the Curti et al. (2017) N2 method, based on the log ([N II] $\lambda 6583/H\alpha$) ratio, to calculate the metallicities presented in our analyses. This facilitates comparison with the largest number of galaxies in our comparison samples, many of which do not have the spectroscopic coverage to use other line ratios. Although all strong-line methods ultimately rely on underlying correlations among parameters, such as ionization and metallicity (e.g., Kewley & Dopita 2002; Nagao et al. 2006), the consistency between our host galaxy sample and SDSS (see Figure 3) suggests that they are similar enough to the calibration sample from Curti et al. (2017) that the use of their N2 diagnostics is reliable. For cases where the uncertainties on the log([N II]/Hα) ratio were larger than the ratios themselves, we instead calculated 1σ upper limits on the line ratio and then calculated 1σ upper limits on the metallicities. One galaxy in our sample, GALEXASC J005328.92−362154.1, does not have a clear detection of [N II] $\lambda 6583$ because it is blended with a very bright Hα line, and we exclude this galaxy from the metallicity analysis.

The current SFR is typically calculated using the Hα line luminosity. As part of the line-measuring process, we also measured the redshifts of the galaxies in our sample, or verified the archival redshifts. For each galaxy, we used our spectroscopic redshift to calculate the luminosity distance, and then calculated the total rest-frame Hα luminosity from the reddening-corrected Hα line flux. We converted this luminosity to an SFR using the Kennicutt (1998) formula. As Kennicutt (1998) adopted a power-law Salpeter (1955) IMF, we multiplied the resulting SFR by 0.7 to convert from a Salpeter (1955) IMF to a Chabrier (2003) IMF, which corrects for the flattening of the IMF below $1 M_\odot$. This is the same procedure used by Hsyu et al. (2018) to calculate SFRs for their low-metallicity, low-mass galaxy sample that we use as a comparison sample in Section 3. After calculating the SFRs of our sample, we also calculate the sSFRs by dividing the SFRs by the stellar masses from the broadband SED fits. For the case of GALEXASC J134316.80 −313318.2, with only an upper limit on its mass, we treat the calculated sSFR as a lower limit.

Though we do not examine luminosity in detail in our analyses, our sample was selected based on a luminosity threshold ($\log L/L_\star \leqslant -1.5$), and we also report the luminosities of our galaxies based on 2MASS (Skrutskie et al. 2006, 2019) K_S-band magnitudes. We collected the K_S-band magnitudes for the galaxies in our sample from the ASAS-SN Bright Supernova Catalogs (Holoien et al. 2017a, 2017c, 2017b) from which our sample was drawn. As the K_S-band magnitude has a well-defined luminosity function (Kochanek et al. 2001), it provides a natural estimate for the stellar luminosities of the galaxies in our sample. In the ASAS-SN catalogs, the authors obtained the 2MASS magnitudes from the 2MASS Extended Source Catalog when available, and from the 2MASS Point Source Catalog when the galaxies were not detected in the Extended Source Catalog. For galaxies not detected in 2MASS but detected in WISE $W1$ data, they estimated the K_S-band magnitude by subtracting the average $K_s - W1$ offset of -0.51 mag calculated from all galaxies detected in both filters. Finally, for galaxies not detected by either 2MASS or WISE, they assumed an upper limit of $K_s > 15.6$, equal to the faintest detected galaxy in their sample. After collecting the K_S apparent magnitudes from the ASAS-SN catalogs, we then converted to absolute magnitudes using the distance moduli calculated from the galaxies' spectroscopic redshifts.

The coordinates, redshifts, distances, masses, metallicities, SFRs, sSFRs, and absolute K_S-band magnitudes of the galaxies in our sample are presented in Table 2. Redshifts that had not been previously measured or that differ from previously reported measurements are noted with an asterisk.

As our sample largely consists of longslit spectra centered on the galaxy nuclei, there is a possibility that the properties we derive from these spectra are not truly "global." Because of this, we performed some checks to verify that the line fluxes and galaxy properties we derive can be robustly compared to other galaxy samples. First, looking at the acquisition images of our spectra, the majority of our sample consists of small galaxies whose light is mostly contained within the slit. Thus, only for a handful of cases is there a chance of significant slit losses. Further, a handful of our sample were observed multiple times, either with different longslit orientations or with both MUSE and one of our longslit instruments. We find that the properties we derive for the galaxies with multiple observations are consistent between observations, implying that we are able to measure galaxy properties robustly with our longslit spectra. We also compared our derived SFRs to the SFRs derived by Brown et al. (2019) from their photometric SED fits, finding that the SFRs we derive from the Hα luminosities are consistent with their SFRs. Finally, we take steps to ensure that our comparison samples are capturing a similar fraction of host light as our longslit spectra, so that they will be directly comparable to our sample (see Section 3).

3. Analysis and Comparison to Other Galaxy Samples

To determine how our SN host galaxies compare to general galaxies, we compare our sample to several samples from literature. Our primary comparison sample is the SDSS DR8 sample (Eisenstein et al. 2011), for which line flux measurements and galaxy property measurements are available in the MPA-JHU value-added catalogs. Because the SDSS catalog values are based on spectra taken with fibers of 2″–3″ diameter, their galaxy properties are not truly "global" properties, as any light outside of the fiber width would not be included. To make their sample more directly comparable to ours, we used only those SDSS galaxies with redshifts of $z < 0.05$, the same redshift range of our sample, so that the area covered by their fibers would be roughly comparable to the area covered by the longslits we used for our spectra. We also only include galaxies with $\log(M_\star/M_\odot) \geqslant 7$, as below this value the line fluxes and derived metallicities are not reliable. These redshift and mass cuts reduce the SDSS sample from 643,727 to 256,529 galaxies.

As the SDSS sample is primarily concentrated toward higher masses and luminosities than our low-luminosity sample, we also selected two low-luminosity samples of galaxies for comparison. The first (Berg et al. 2012; hereafter, B12) consists of longslit spectroscopic observations of H II regions from 42

Table 2
Physical Properties of Our Low-L SN Ia Host Galaxy Sample

Galaxy Name[a]	SN Name	Redshift[b]	Distance (Mpc)	$\log(M_\star)$ $(M_\odot)$	$12 + \log(\mathrm{O/H})$[c]	$\log(\mathrm{SFR})$ $M_\odot\,\mathrm{yr}^{-1}$	$\log(\mathrm{sSFR})$ Gyr^{-1}	M_{K_S}[d]
2MASX J03051061	ASASSN-15ti	0.0172	75.1	$8.72^{+0.04}_{-0.04}$	$8.45^{+0.01}_{-0.01}$	$-0.87^{+0.01}_{-0.01}$	$-0.59^{+0.05}_{-0.05}$	-18.18 ± 0.20
AGC 331536	ASASSN-16ke	0.028	123.0	$8.60^{+0.28}_{-0.11}$	$8.49^{+0.02}_{-0.02}$	$-2.21^{+0.02}_{-0.02}$	$-1.81^{+0.13}_{-0.30}$	-17.26 ± 0.11
APMUKS(BJ) B032028.93	ASASSN-16dx	0.0295	130.0	$8.05^{+0.60}_{-0.17}$	$8.47^{+0.01}_{-0.01}$	$-0.64^{+0.01}_{-0.01}$	$0.310^{+0.18}_{-0.61}$	-18.37 ± 0.20
CGMW 2-2125	ASASSN-16jq	0.018	78.6	$9.10^{+0.36}_{-0.16}$	$8.62^{+0.12}_{-0.10}$	$-2.08^{+0.11}_{-0.15}$	$-2.18^{+0.27}_{-0.51}$	> -18.88
ESO 113-G047	ASASSN-14me	0.018	78.6	$8.46^{+0.62}_{-1.13}$	$8.35^{+0.02}_{-0.02}$	$-0.54^{+0.01}_{-0.01}$	$-0.00^{+0.01}_{-0.63}$	-17.19 ± 0.11
ESO 357-G005	ASASSN-15pz	0.0149	64.9	$7.28^{+0.86}_{-0.34}$	$8.65^{+0.13}_{-0.10}$	$-2.34^{+0.11}_{-0.14}$	$-0.62^{+0.45}_{-1.00}$	-16.67 ± 0.11
ESO 466-G032	2016ekg	0.0171	74.6	$8.79^{+0.03}_{-0.05}$	$8.56^{+0.01}_{-0.01}$	$-2.15^{+0.01}_{-0.01}$	$-1.94^{+0.06}_{-0.04}$	-18.16 ± 0.20
ESO 509-IG064	ASASSN-16hp	0.008663	37.6	$8.57^{+0.01}_{-0.05}$	$8.46^{+0.00}_{-0.00}$	$-1.49^{+0.01}_{-0.01}$	$-1.06^{+0.06}_{-0.02}$	-17.88 ± 0.10
GALEXASC J000802.78	ASASSN-15rq	0.0236	104.0	$8.43^{+0.70}_{-0.67}$	$8.47^{+0.04}_{-0.04}$	$-1.29^{+0.04}_{-0.04}$	$-0.72^{+0.71}_{-0.74}$	-17.38 ± 0.11

Notes. Physical parameters for the galaxies in our sample. Descriptions of how each property was calculated are given in Section 2.3. A portion of the table is shown here for guidance regarding its form and content; the full table is available in machine-readable format in the online journal.
[a] For cases where a galaxy has not been previously cataloged by any survey, and thus does not have an archival name or designation, we use "Uncatalogued" for the name. Some galaxy names are abbreviated here to prevent the width of the table from extending beyond the page, but full names are given in the version of the table available in the online journal.
[b] Redshifts that had not been previously measured or that differ substantially from archival measurements are denoted with an asterisk.
[c] Metallicities are calculated using the N2 method of Curti et al. (2017).
[d] K_S-band magnitudes are taken from the 2MASS catalogs when available, or calculated from the WISE $W1$-band magnitudes when not. If the galaxy is not detected in either catalog, we assume an upper limit of $m_{K_S} > 15.6$, as described in the text.

(This table is available in its entirety in machine-readable form.)

low-luminosity galaxies in the Spitzer Local Volume Legacy (LVL) survey. The second (Hsyu et al. 2018; hereafter, H18) consists of longslit spectroscopic observations of 45 low-metallicity blue compact dwarf galaxies selected from SDSS DR12 (Alam et al. 2015). Although the latter sample was selected for low metallicity rather than luminosity, these systems are also low-mass and low-luminosity. As both samples use longslit spectra with similar slit widths as our data, we do not perform any additional corrections to make them comparable to our sample.

For the SDSS sample, we used the stellar masses and SFRs from the MPA-JHU catalog and calculated the sSFRs using those. As the MPA-JHU catalogs used a Kroupa (2001) IMF to calculate the masses and SFRs, we converted their measurements to a Salpeter (1955) IMF by multiplying them by a factor of 1.5 (Brinchmann et al. 2004), then converted the SFRs to a Chabrier (2003) IMF by multiplying by 0.7, so that they would be directly comparable to the other samples. Though the MPA-JHU sample is the largest of the four samples we compare, we elected to convert all our samples to a Chabrier (2003) IMF, as this has been proven to be accurate for low-mass, low-luminosity samples like ours (e.g., that of H18). It is also only a minor correction, as the Kroupa (2001) and Chabrier (2003) IMFs are quite similar. For the B12 sample, we used the masses from their paper. As their paper provided spectra of H II regions, rather than of the galaxies as a whole, we were unable to use the reported Hα fluxes to calculate the Hα luminosities and SFRs for the galaxies. Instead, we use the Hα luminosities for the LVL galaxies from Kennicutt & Lee (2008) to calculate the SFRs and sSFRs of the B12 sample.[25] For galaxies in the B12 sample with multiple spectra of H II regions, we use the same SFRs and masses and calculate the metallicities for each H II region separately. Kennicutt & Lee (2008) do not give uncertainties for the Hα luminosities in their sample, and

instead give a range of ±0.07–0.15 dex, based on the typical uncertainties on the distances to the galaxies. We assume an uncertainty of 0.15 dex on $L_{\mathrm{H}\alpha}$, the upper end of their specified range, when calculating SFRs for galaxies in the B12 sample. Finally, for the H18 sample, we obtained masses and SFRs from their paper.

For all three samples, we used the [N II] $\lambda6583$ and Hα fluxes to calculate the Curti N2 metallicities, as we did for our sample. We calculated upper limits on the metallicities when the [N II] $\lambda6583$ and Hα lines were not robustly detected.

Figure 4 shows the distribution of our sample and the comparison samples in stellar mass and metallicity. As has been found for SN Ia host galaxies in the past (e.g., Childress et al. 2013), our galaxies do not clearly stand out from the other galaxy samples. They largely fall on the low-M, low-metallicity tail of the distribution of the SDSS sample and overlap with the higher-metallicity galaxies from the B12 sample. The H18 sample is largely lower in mass and metallicity than our sample, but this is unsurprising, given that it was specifically selected to be low metallicity.

Five of the six lowest-mass galaxies in our sample have metallicities that appear high for their masses, and we flagged these as potential outliers. These galaxies are: ESO 357-G005 (ASASSN-15pz), GALEXASC J063224.91−713403.9 (OGLE16dha), GALEXASC J010647.95−465904.1 (ASASSN-14lw), UGCA 430 (ASASSN-16jf), and the uncatalogued host of ASASSN-15fy. We highlight these five galaxies using purple outlines in Figure 4.

To test whether these galaxies truly have abnormally high metallicities when compared to the rest of our sample and the comparison samples, we fit all of the low-L samples with a linear equation of the form

$$12 + \log(\mathrm{O/H}) = a(\log(M_\star/M_\odot) - \mu_M) + b, \quad (1)$$

where a is the slope, b is the intercept, and μ_M is the mean log $(M_\star)$ of the sample being fit. We pivot the relations on the mean in order to make the uncertainties on the a and b parameters

---

[25] Four of the galaxies in the B12 sample do not have Hα luminosities in Kennicutt & Lee (2008), and we exclude these from our analyses of SFR and sSFR.
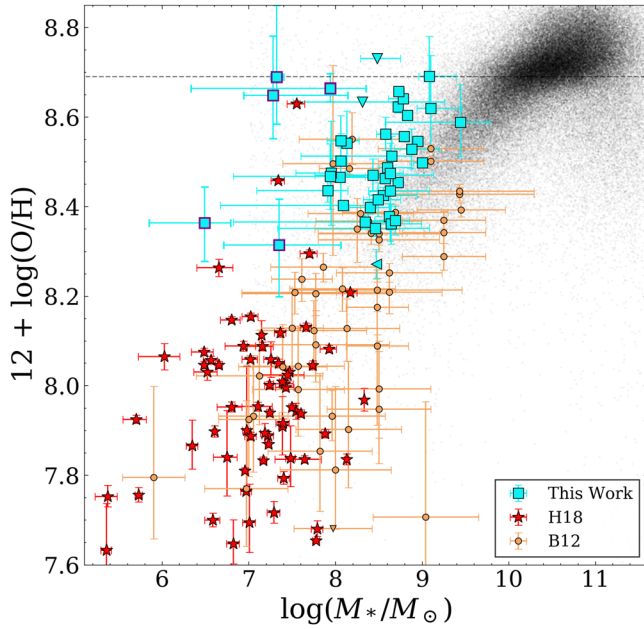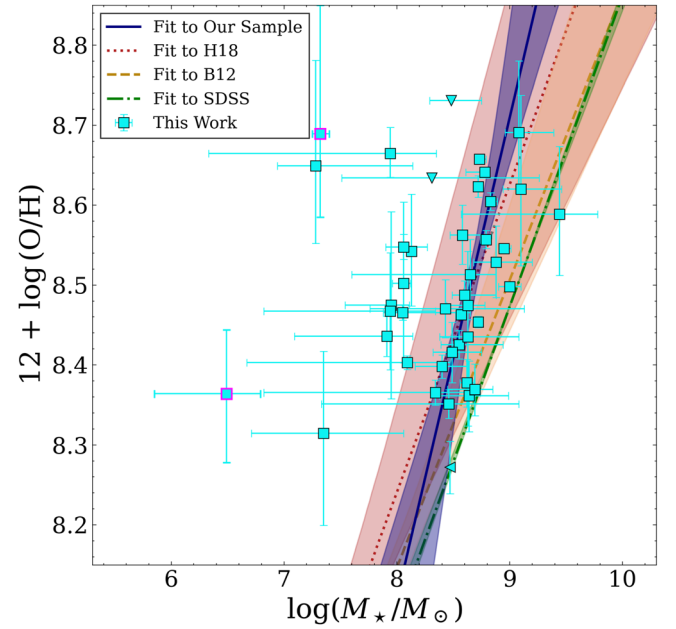
Figure 4. Stellar masses and Curti N2 metallicities for our SN Ia host galaxy sample (blue squares) compared to the low-L galaxy samples of B12 (yellow circles) and H18 (red stars). SDSS DR8 galaxies are shown in black. 1σ upper limits in metallicity are shown as downward-facing triangles and upper limits in mass are shown as leftward-facing triangles. The five galaxies highlighted with a purple outline indicate the five very-low-mass galaxies we identified as potential outliers, with particularly high metallicities for their masses. The horizontal dashed line indicates Solar metallicity, $Z_\odot = 8.69$ (Asplund et al. 2009).

Figure 5. Stellar masses and Curti N2 metallicities for our SN Ia host galaxy sample (blue squares) compared to linear M–Z fits to our sample (navy), the B12 sample (yellow), the H18 sample (red), and the SDSS sample (green). The shaded regions in matching colors show the 1σ range for each fit. Note the change in scales compared to Figure 4, which we have adjusted to more clearly focus on our sample. The two data points highlighted in magenta are 3σ outliers from all four M–Z fits.

essentially uncorrelated. To robustly measure the fit and estimate the uncertainties on the a and b parameters, we use bootstrap resampling with 15,000 iterations. We find $(a, b)_{\rm us} = (0.60^{+0.37}_{-0.15}, 8.34^{+0.37}_{-0.13})$ for our sample, where the best-fit value is the median of our bootstrapped values and the errors are 1σ uncertainties. For the B12, H18, and SDSS samples, we find $(a, b)_{\rm B12} = (0.36^{+0.09}_{-0.06}, 8.21^{+0.04}_{-0.04})$, $(a, b)_{\rm H18} = (0.38^{+0.15}_{-0.09}, 7.88^{+0.05}_{-0.07})$, and $(a, b)_{\rm SDSS} = (0.39^{+0.01}_{-0.02}, 8.53^{+0.01}_{-0.01})$ respectively. For the SDSS fit, we only include those galaxies with $\log(M_\star/M_\odot) \leqslant 9.7$, to exclude the galaxies with masses above the scale where the slope of the relation becomes shallower.

In Figure 5, we show our sample as well as the best-fit lines and 1σ uncertainties for all four galaxy samples. All three fits are generally quite consistent through the mass range shown, particularly those for the B12 and H18 samples. We find that of the five points we identified as having potentially high metallicities, only two, UGCA 430 and the host of ASASSN-15fy, are outliers from all four fits at the 3σ level. We highlight these two points in magenta in Figure 5. With only two true outliers, we thus conclude that there is no significant evidence from our sample that the lowest-mass SN Ia host galaxies are more metal-rich than typical low-mass galaxies.

However, while not individually significant, there seem to be an excess of galaxies that are metal-rich for their masses, with 10 of the 14 lowest-mass galaxies lying $\sim 1\sigma$ above all but the H18 trend line. Further, none of our galaxies have low metallicities for their masses. Some of this is in part due to our sample selection method, removing higher-mass galaxies, rather than a lack of these types of galaxies in general. However, there is weak evidence that low-mass SN Ia host galaxies may be more enriched than their non-SN-host counterparts.

We also looked at other properties of our sample and the comparison samples to examine whether there are any other characteristics for which the two 3σ outliers are unique, or whether our sample stands out. Figure 6 shows the stellar masses of our sample and the comparison samples compared to their current SFRs. The magenta line in the figure corresponds to $\log({\rm sSFR}) < -11$, and is the division used by Brown et al. (2019) to separate actively star-forming and passive galaxies. As expected, based on their locations in the diagnostic diagrams of Figure 3, the majority of our galaxies lie above this dividing line, implying that they are actively star-forming. The six galaxies below the line are all very close to the dividing line, and of these, only four are inconsistent with being above the line, given the uncertainties on their masses and SFRs. Our sample does not clearly stand out from any of our comparison samples, and is quite similar to the B12 sample, in particular. The two galaxies noted as having high metallicities for their masses are again highlighted in magenta in the figure. While they do have some of the lower SFRs of the galaxies in our sample, they do not stand out from the other galaxies. We conclude that there is nothing atypical about the SFRs of our sample, given their masses.

In Figure 7, we show the SFRs and metallicities of our sample. Our galaxies tend to have higher metallicities than the galaxies with similar SFRs in our low-L comparison samples, but are generally consistent with the outer edge of the SDSS sample. There is little overlap between our sample and the H18 sample, while the B12 sample is fairly evenly spread throughout the region spanned by our sample and the H18 sample. There is no clear trend in metallicity with SFR for the three low-L samples shown here, with the metallicity spread for each sample being fairly flat over a wide range of SFRs. The two high-metallicity galaxies noted in magenta do not stand out from the rest of the galaxies in our sample in the SFR–metallicity plane.
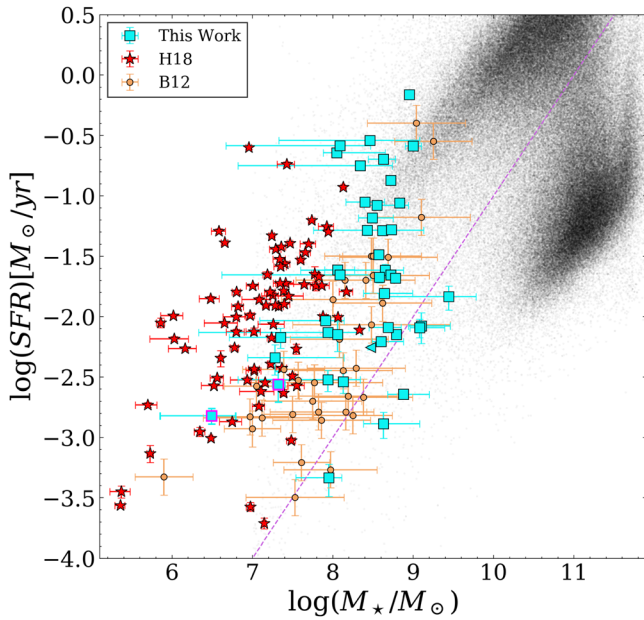
Figure 6. The stellar masses and SFRs of our sample compared to our comparison samples. The colors and symbols match those of Figure 4, with the two points highlighted with magenta outlines indicating the two galaxies with notably high metallicities for their masses. The magenta dashed line shows the division between actively star-forming galaxies and passive galaxies, as defined in Brown et al. (2019), corresponding to log(sSFR)< −11.

Figure 7. The SFRs and Curti N2 metallicities for our sample compared to our galaxy comparison samples. The colors and symbols match those of Figure 4, with the two points highlighted with magenta outlines indicating the two galaxies with notably high metallicities for their masses. 1σ upper limits in metallicity are shown as downward-facing triangles.

In Figure 8, we examine the sSFRs of our sample and comparison samples compared to their metallicities. We again see that our sample is higher in metallicity compared to the other low-L samples, with even less overlap between our sample and the B12 and H18 samples than in the space of SFR and metallicity. Our sample is again generally consistent with the SDSS DR8 sample, however. We again highlight the two galaxies identified as having high metallicities for their masses, and note that they do not seem to have atypical metallicities, given their sSFRs, with one falling in the area of the figure most densely populated by SDSS galaxies. Where our galaxies show no obvious trend in metallicity with increasing sSFR, as was the case with SFR, this does not appear to be true for the other low-L samples. The B12 sample has a clear trend, with the metallicity decreasing as sSFR increases. While the H18 sample does not have as clear a trend overall, we note that the highest-metallicity galaxies in the H18 sample tend to have higher sSFRs.

For both SFR and sSFR, our sample does not appear to be particularly metal-rich or metal-poor compared to the general population of galaxies from SDSS. In comparison to similar low-L samples in B12 and H18, however, our sample is more enriched for a given SFR/sSFR. Neither SFR nor sSFR appear to have a clear correlation with metallicity in our sample, despite there being a trend with mass.

4. Discussion

Our spectroscopic examination of 44 low-luminosity host galaxies of SNe Ia indicates that this population of galaxies is similar to typical galaxies in metallicity, SFR, sSFR, and stellar mass. In particular, the SFRs and sSFRs of our sample appear to be quite normal, given the galaxies' masses and metallicities. These results support the conclusions of previous examinations of SN Ia host galaxies (e.g., Childress et al. 2013), which have
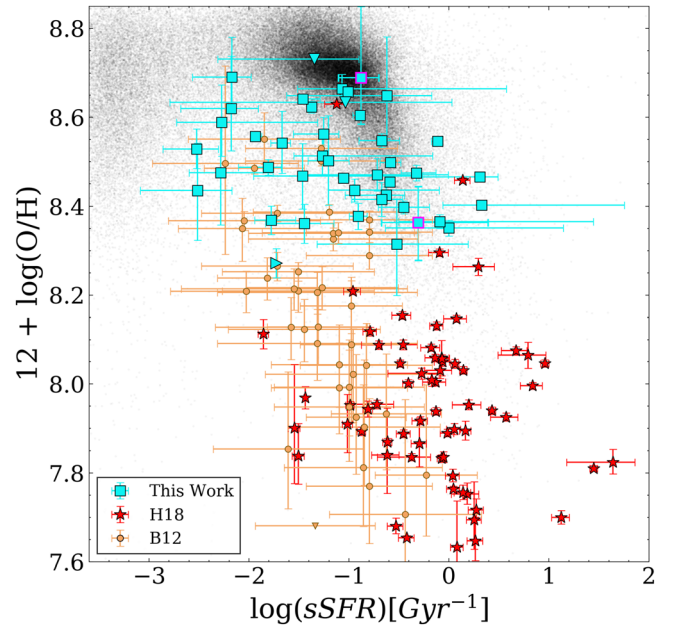
Figure 8. The sSFRs and Curti N2 metallicities of our sample compared to the comparison samples. The colors and symbols match those of Figure 4, with the two points highlighted with magenta outlines indicating the two galaxies with notably high metallicities for their masses. 1σ upper limits in metallicity are shown as downward-facing triangles and lower limits in sSFR are shown as right-facing triangles.

found that SN Ia hosts generally have metallicites similar to galaxies of the same masses and SFRs.

While 10 of the 14 least massive galaxies in our sample lie $\sim 1\sigma$ above the mass–metallicity relations defined by our comparison galaxy samples (which are generally consistent with one another, and with the M–Z relation defined by our entire sample), we find that only two of these are inconsistent

with all the fits at the 3σ level. These two galaxies do not appear to be outliers when looking at the mass–SFR, SFR–metallicity, or sSFR–metallicity planes. Both galaxies host normal SNe Ia, indicating that there does not appear to be a correlation between the subtype of the SN and the host having a high metallicity in our sample.

This conclusion is not without caveats, however. First, while we have taken steps to ensure that our sample of longslit and IFU spectra are comparable to one another and to the comparison samples we use, in some cases our longslit spectra do not capture all of the host galaxy light. This would result in some inaccuracies of the properties we derive for our galaxies, such as SFR and metallicity, which are based on spectroscopic line fluxes. As mentioned in Sections 2.1 and 2.3, we have checked our results for consistency using some galaxies with multiple observations in our sample and by comparing our spectroscopically derived SFRs to the photometrically derived ones from Brown et al. (2019), and find that our results are consistent. We thus believe the effects of slit losses on our conclusions are minimal.

A second point to note is that the galaxies in our sample are all very low redshift, and that one should not assume our conclusions will apply at higher redshifts. However, the B12 and H18 samples are similarly low redshift, and we have used a redshift cut on the MPA-JHU sample, so there is no concern that our comparisons to these samples are biased by differences in distance. It is presently difficult to observe these dwarf galaxies at significantly higher redshifts. As more facilities that can make these observations become available in the future, it will be important to expand to higher redshifts to examine whether younger low-luminosity SN Ia hosts show more significant differences.

A more substantial caveat with our conclusions is the size of our sample. Though our sample contains more low-luminosity galaxies than previous SN Ia host samples, it only includes nine galaxies with $\log(M_\star/M_\odot) < 8$, where we see any evidence for outliers from the mass–metallicity relations, in the sense that the lowest-mass galaxies do generally lie above the mass–metallicity relations. Larger samples of low-luminosity and low-mass SN Ia host galaxies, particularly those with $\log(M_\star/M_\odot) < 8$, are needed to determine if this pattern is robust.

If our results are correct, this would have promising implications for both SN studies and host galaxy studies. Studies of SN host galaxies often use photometry to infer the physical properties of the galaxies being studied, as photometry typically requires significantly less observational resources than spectroscopy. While methods such as photometric SED fitting can obtain fairly reliable masses and even SFRs, metallicity is typically estimated using a mass–metallicity relation, and cannot be measured directly without spectroscopy. If low-luminosity SN Ia hosts do not deviate from standard mass–metallicity relations, the inferred metallicities for these galaxies would be trustworthy. It is thus important to determine whether the consistency of our sample with general galaxy samples is seen in additional data sets, and to correct metallicity studies of SN Ia host galaxies if not.

These findings may impact our understanding of SNe Ia as well. It has previously been seen that higher host galaxy metallicity results in brighter, faster-declining, and redder SNe Ia (e.g., Howell et al. 2009; Pan et al. 2014). However, these have typically also been more massive and older hosts in previous samples, and our sample indicates that host metallicity does not appear to be the primary attribute regulating SN

properties, as the outliers in host metallicity host normal SNe Ia. Examination of the SN Ia rate and SN Ia properties in this low-luminosity population of hosts could thus have implications on our understanding of SN Ia progenitor systems and how the metallicity of the progenitor affects the SN explosion. This in turn could also affect cosmological studies based on SNe Ia.

Apart from providing important evidence that low-luminosity, low-mass SN Ia host galaxies are consistent in metallicity with general galaxies, this work provides the spectroscopic observations needed to perform studies on specific SN Ia rates and SN property–host property correlations, as described above. In future work, we will combine this sample with the much larger sample of more luminous and massive ASAS-SN SN Ia host galaxies that have archival spectroscopic observations. This will allow for a comprehensive study of how the host environment affects the SN Ia progenitors and explosions in the low-redshift Universe, which will include a substantial fraction of low-luminosity hosts for the first time.

ORCID iDs

Thomas W.-S. Holoien ⓘ https://orcid.org/0000-0001-9206-3460
Vera L. Berger ⓘ https://orcid.org/0000-0002-7303-8144
Jason T. Hinkle ⓘ https://orcid.org/0000-0001-9668-2920
L. Galbany ⓘ https://orcid.org/0000-0002-1296-6887
Allison L. Strom ⓘ https://orcid.org/0000-0001-6369-1636
Joseph P. Anderson ⓘ https://orcid.org/0000-0003-0227-3451
K. D. French ⓘ https://orcid.org/0000-0002-4235-7337
Christopher S. Kochanek ⓘ https://orcid.org/0000-0001-6017-2961
Hanindyo Kuncarayakti ⓘ https://orcid.org/0000-0002-1132-1366
Joseph D. Lyman ⓘ https://orcid.org/0000-0002-3464-0642
Nidia Morrell ⓘ https://orcid.org/0000-0003-2535-3091
Jose L. Prieto ⓘ https://orcid.org/0000-0003-0943-0026
Sebastián F. Sánchez ⓘ https://orcid.org/0000-0001-6444-9307
Gregory L. Walth ⓘ https://orcid.org/0000-0002-6313-6808

References

Alam, S., Albareti, F. D., Allende Prieto, C., et al. 2015, ApJS, 219, 12
Aldering, G., Adam, G., Antilogus, P., et al. 2002, Proc. SPIE, 4836, 61
Anderson, J. P., James, P. A., & Förster, F., et al. 2015, MNRAS, 448, 732
Asplund, M., Grevesse, N., Sauval, A. J., & Scott, P. 2009, ARA&A, 47, 481
Bacon, R., Vernet, J., Borisova, E., et al. 2014, Msngr, 157, 13
Baldwin, J. A., Phillips, M. M., & Terlevich, R. 1981, PASP, 93, 5
Bellm, E. C., Kulkarni, S. R., Graham, M. J., et al. 2019, PASP, 131, 018002
Bennett, C. L., Larson, D., Weiland, J. L., & Hinshaw, G. 2014, ApJ, 794, 135
Berg, D. A., Skillman, E. D., Marble, A. R., et al. 2012, ApJ, 754, 98
Branch, D., & van den Bergh, S. 1993, AJ, 105, 2231
Brinchmann, J., Charlot, S., White, S. D. M., et al. 2004, MNRAS, 351, 1151
Brown, J. S., Stanek, K. Z., Holoien, T. W.-S., et al. 2019, MNRAS, 484, 3785
Bruzual, G., & Charlot, S. 2003, MNRAS, 344, 1000
Cappellari, M. 2012, pPXF: Penalized Pixel-Fitting stellar kinematics extraction, Astrophysics Source Code Library, ascl:1210.002
Cappellari, M. 2017, MNRAS, 466, 798
Cappellari, M., & Emsellem, E. 2004, PASP, 116, 138
Cardelli, J. A., Clayton, G. C., & Mathis, J. S. 1989, ApJ, 345, 245
Chabrier, G. 2003, PASP, 115, 763
Chambers, K. C., Magnier, E. A., Metcalfe, N., et al. 2016, arXiv, arXiv:1612.05560
Childress, M., Aldering, G., Antilogus, P., et al. 2013, ApJ, 770, 107
Cid Fernandes, R., Stasińska, G., Mateus, A., & Vale Asari, N. 2011, MNRAS, 413, 1687
Curti, M., Cresci, G., Mannucci, F., et al. 2017, MNRAS, 465, 1384
Dressler, A., Bigelow, B., Hare, T., et al. 2011, PASP, 123, 288
Eisenstein, D. J., Weinberg, D. H., Agol, E., et al. 2011, AJ, 142, 72
Filippenko, A. V. 1989, PASP, 101, 588
Filippenko, A. V., Richmond, M. W., Branch, D., et al. 1992a, AJ, 104, 1543
Filippenko, A. V., Richmond, M. W., Matheson, T., et al. 1992b, ApJL, 384, L15
Flewelling, H. A., Magnier, E. A., Chambers, K. C., et al. 2020, ApJS, 251, 7
Foley, R. J., Challis, P. J., Chornock, R., et al. 2013, ApJ, 767, 57
Gaia Collaboration, Brown, A. G. A., Vallenari, A., et al. 2021, A&A, 649, A1
Galbany, L., Anderson, J. P., Rosales-Ortega, F. F., et al. 2016, MNRAS, 455, 4087
Galbany, L., Anderson, J. P., Sánchez, S. F., et al. 2018, ApJ, 855, 107
Galbany, L., Stanishev, V., Mourão, A. M., et al. 2014, A&A, 572, A38
Gallagher, J. S., Garnavich, P. M., Berlind, P., et al. 2005, ApJ, 634, 210
Gallagher, J. S., Garnavich, P. M., Caldwell, N., et al. 2008, ApJ, 685, 752
Hamuy, M., Phillips, M. M., Suntzeff, N. B., et al. 1996, AJ, 112, 2391
Hamuy, M., Trager, S. C., Pinto, P. A., et al. 2000, AJ, 120, 1479
Holoien, T. W.-S., Brown, J. S., Stanek, K. Z., et al. 2017a, MNRAS, 471, 4966
Holoien, T. W.-S., Brown, J. S., Stanek, K. Z., et al. 2017b, MNRAS, 467, 1098
Holoien, T. W.-S., Stanek, K. Z., Kochanek, C. S., et al. 2017c, MNRAS, 464, 2672

Howell, D. A., Sullivan, M., Brown, E. F., et al. 2009, ApJ, 691, 661
Hsyu, T., Cooke, R. J., Prochaska, J. X., & Bolte, M. 2018, ApJ, 863, 134
Jones, D. O., Riess, A. G., & Scolnic, D. M. 2015, ApJ, 812, 31
Jones, D. O., Riess, A. G., Scolnic, D. M., et al. 2018, ApJ, 867, 108
Kauffmann, G., Heckman, T. M., Tremonti, C., et al. 2003, MNRAS, 346, 1055
Kelsey, L., Sullivan, M., Smith, M., et al. 2021, MNRAS, 501, 4861
Kelz, A., Verheijen, M. A. W., Roth, M. M., et al. 2006, PASP, 118, 129
Kennicutt, R. C. J. 1998, ARA&A, 36, 189
Kennicutt, R C. J., & Lee, J. C. 2008, ApJS, 178, 247
Kewley, L. J., & Dopita, M. A. 2002, ApJS, 142, 35
Kewley, L. J., Dopita, M. A., Sutherland, R. S., Heisler, C. A., & Trevena, J. 2001, ApJ, 556, 121
Kewley, L. J., & Ellison, S. L. 2008, ApJ, 681, 1183
Kewley, L. J., Groves, B., Kauffmann, G., & Heckman, T. 2006, MNRAS, 372, 961
Kim, Y.-L., Kang, Y., & Lee, Y.-W. 2019, JKAS, 52, 181
Kim, Y.-L., Smith, M., Sullivan, M., & Lee, Y.-W. 2018, ApJ, 854, 24
Kistler, M. D., Stanek, K. Z., Kochanek, C. S., Prieto, J. L., & Thompson, T. A. 2013, ApJ, 770, 88
Kochanek, C. S., Pahre, M. A., Falco, E. E., et al. 2001, ApJ, 560, 566
Kriek, M., van Dokkum, P. G., Labbé, I., et al. 2009, ApJ, 700, 221
Kroupa, P. 2001, MNRAS, 322, 231
Lampeitl, H., Smith, M., Nichol, R. C., et al. 2010, ApJ, 722, 566
Leibundgut, B., Kirshner, R. P., Phillips, M. M., et al. 1993, AJ, 105, 301
Li, W. D., Filippenko, A. V., Treffers, R. R., et al. 2000, in AIP Conf. Ser. 522, ed. S. S. Holt & W. W. Zhang (Melville, NY: AIP), 103
Maoz, D., & Graur, O. 2017, ApJ, 848, 25
Maoz, D., Mannucci, F., & Brandt, T. D. 2012, MNRAS, 426, 3282
Moreno-Raya, M. E., López-Sánchez, Á. R., & Mollá, M. 2016a, MNRAS, 462, 1281
Moreno-Raya, M. E., Mollá, M., & López-Sánchez, Á. R. 2016b, ApJL, 818, L19
Nagao, T., Maiolino, R., & Marconi, A. 2006, A&A, 459, 85
Neill, J. D., Sullivan, M., Howell, D. A., et al. 2009, ApJ, 707, 1449
Nomoto, K., Kobayashi, C., & Tominaga, N. 2013, ARA&A, 51, 457
Osterbrock, D. E. 1989, Astrophysics of Gaseous Nebulae and Active Galactic Nuclei (Sausalito, CA: Univ. Science Books)
Pan, Y.-C., Sullivan, M., Maguire, K., et al. 2014, MNRAS, 438, 1391
Perlmutter, S., Aldering, G., Goldhaber, G., et al. 1999, ApJ, 517, 565
Phillips, M. M. 1993, ApJL, 413, L105
Phillips, M. M., Wells, L. A., Suntzeff, N. B., et al. 1992, AJ, 103, 1632
Pogge, R. W., Atwood, B., Brewer, D. F., et al. 2010, Proc. SPIE, 7735, 77350A
Ponder, K. A., Wood-Vasey, W. M., Weyant, A., et al. 2021, ApJ, 923, 197
Popovic, B., Brout, D., Kessler, R., Scolnic, D., & Lu, L. 2021, ApJ, 913, 49
Riess, A. G., Filippenko, A. V., Challis, P., et al. 1998, AJ, 116, 1009
Rigault, M., Aldering, G., Kowalski, M., et al. 2015, ApJ, 802, 20
Rigault, M., Brinnel, V., Aldering, G., et al. 2020, A&A, 644, A176
Rigault, M., Copin, Y., Aldering, G., et al. 2013, A&A, 560, A66
Roman, M., Hardin, D., Betoule, M., et al. 2018, A&A, 615, A68
Rose, B. M., Garnavich, P. M., & Berg, M. A. 2019, ApJ, 874, 32
Roth, M. M., Kelz, A., Fechner, T., et al. 2005, PASP, 117, 620
Salpeter, E. E. 1955, ApJ, 121, 161
Schlafly, E. F., & Finkbeiner, D. P. 2011, ApJ, 737, 103
Shappee, B. J., Holoien, T. W.-S., Drout, M. R., et al. 2019, ApJ, 870, 13
Shappee, B. J., Piro, A. L., Stanek, K. Z., et al. 2018, ApJ, 855, 6
Shappee, B. J., Prieto, J. L., Grupe, D., et al. 2014, ApJ, 788, 48
Shappee, B. J., Stanek, K. Z., Kochanek, C. S., & Garnavich, P. M. 2017, ApJ, 841, 48
Skrutskie, M. F., Cutri, R. M., Stiening, R., et al. 2006, AJ, 131, 1163
Skrutskie, M. F., Cutri, R. M., Stiening, R., et al. 2019, 2MASS All-Sky Point Source Catalog, IPAC, doi:10.26131/IRSA2
Smith, M., Sullivan, M., Wiseman, P., et al. 2020, MNRAS, 494, 4426
Sullivan, M., Conley, A., Howell, D. A., et al. 2010, MNRAS, 406, 782
Tonry, J. L., Denneau, L., Heinze, A. N., et al. 2018, PASP, 130, 064505
Tucker, M. A., Shappee, B. J., Vallely, P. J., et al. 2020, MNRAS, 493, 1044
Uddin, S. A., Burns, C. R., Phillips, M. M., et al. 2020, ApJ, 901, 143
Uddin, S. A., Mould, J., & Wang, L. 2017, ApJ, 850, 135
Vallely, P. J., Fausnaugh, M., Jha, S. W., et al. 2019, MNRAS, 487, 2372
Veilleux, S., & Osterbrock, D. E. 1987, ApJS, 63, 295
Verheijen, M. A. W., Bershady, M. A., Andersen, D. R., et al. 2004, AN, 325, 151
Wright, E. L. 2006, PASP, 118, 1711
Wright, E. L., Eisenhardt, P. R. M., Mainzer, A. K., et al. 2010, AJ, 140, 1868
Wright, E. L., Eisenhardt, P. R. M., Mainzer, A. K., et al. 2019, AllWISE Source Catalog, IPAC, doi:10.26131/IRSA1